Redox Thermodynamics of the Ferric−Ferrous Couple of Wild-Type *Synechocystis* KatG and KatG(Y249F)†

Marzia Bellei,‡ Christa Jakopitsch,§ Gianantonio Battistuzzi,‡ Marco Sola,*,‡ and Christian Obinger*,§

Department of Chemistry, University of Modena and Reggio Emilia, via Campi 183, 41100 Modena, Italy, and Department of Chemistry, Division of Biochemistry, BOKU−University of Natural Resources and Applied Life Sciences, Muthgasse 18, A-1190 Vienna, Austria

Received September 7, 2005; Revised Manuscript Received February 24, 2006

ABSTRACT: Crystal structures and mass spectrometric analyses of catalase-peroxidases (KatGs) from different organisms revealed the existence of a peculiar distal Met-Tyr-Trp cross-link. The adduct appears to be important for the catalase but not the peroxidase activity of bifunctional KatG. To examine the effect of the adduct on enzyme redox properties and functions, we have determined the thermodynamics of ferric reduction for wild-type KatG and KatG(Y249F), whose tyrosine-to-phenylalanine mutation prevents cross-link formation. At 25 °C and pH 7.0, the reduction potential of wild-type KatG is found to be −226 ± 10 mV, remarkably lower than the published literature values. The reduction potential of KatG(Y249F) is very similar (−222 ± 10 mV), but variable temperature experiments revealed compensatory differences in reduction enthalpies and entropies. In both proteins, the oxidized state is enthalpically stabilized over the reduced state, but entropy is lost on reduction, which is in strong contrast to horseradish peroxidase, which also features a much more pronounced enthalpic stabilization of the ferriheme. With both proteins, the midpoint potential increased linearly with decreasing pH. We discuss whether the observed redox thermodynamics reflects the differences in structure and function between bifunctional KatG and monofunctional peroxidases.

The four available crystal structures of catalase-peroxidases (KatGs[11]) of *Haloarcula marismortui* (1ITK), *Burkholderia pseudomallei* (1MWV), *Mycobacterium tuberculosis* (1SJ2), and *Synechococcus* PCC 7942 (1UB2) (*1*−*4*) revealed that the organization of their active site is similar to those of cytochrome *c* peroxidase (C*c*P) (*5*) and ascorbate peroxidase (APX) (*6*). In particular, the coordinates of the heme *b* moiety and the distal and proximal triads W122, H123, R119 and D402, H290, and W341 (*Synechocystis* numbering) are almost identical (Figure 1). However, electron density maps demonstrated the presence of a peculiar KatG-specific covalent link between the $C^{\eta 2}$ of distal W122 and $C^{\epsilon 1}$ of Y249 and between $C^{\epsilon 2}$ of Y249 and S^{δ} of M275 (*1*−*4*). This cross-link adds KatG to a growing list of metalloenzymes that have aromatic amino acids covalently modified in their active sites. Recently, mass spectrometric analyses confirmed the existence of this novel adduct in solution (*7*, *8*), and its autocatalytic formation has been demonstrated (*9*).

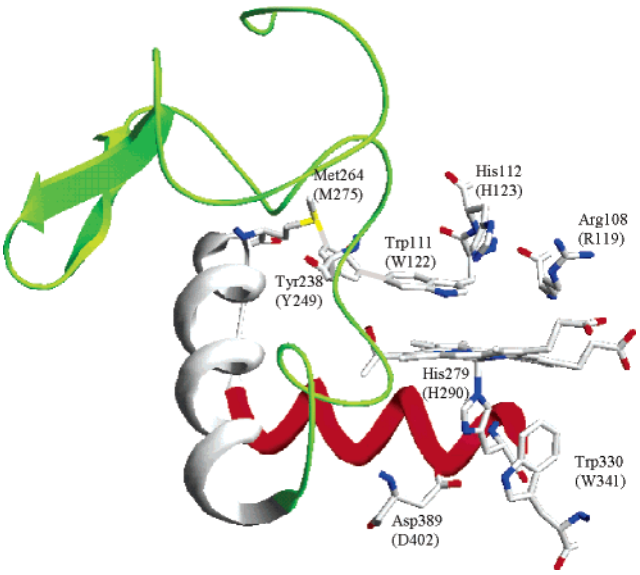

FIGURE 1: Active-site residues of catalase-peroxidase from *Burkholderia pseudomallei* (*Synechocystis* numbers in parentheses). Green, large loop 1 (LL1); gray, helix E; and red, helix F. The Figure was constructed using the coordinates deposited in the protein data bank (accession code 1MWV).

In catalase-peroxidases, the catalatic activity dominates over the peroxidatic reaction. Together with homologous cytochrome *c* peroxidase (C*c*P) and ascorbate peroxidase (APX), KatGs are members of class I of the plant peroxidase superfamily, but neither C*c*P nor APX can oxidize hydrogen

† This work was supported by the Austrian Science Fund (Project Number P18751).

* To whom correspondence should be addressed. Tel: +43-1-36006-6073. Fax: +43-1-36006-6059. E-mail: christian.obinger@boku.ac.at (C.O.); Tel: +39-59-2055037. Fax: +39-59-3735543. E-mail: sola.marco@unimore.it (M.S.).

‡ University of Modena and Reggio Emilia.

§ BOKU−University of Natural Resources and Applied Life Sciences.

[1] [1]Abbreviations: KatG, catalase-peroxidase; C*c*P, cytochrome *c* peroxidase; APX, ascorbate peroxidase; HRP, horseradish peroxidase; $E^{\circ\prime}$, reduction potential, referred to the standard hydrogen electrode, measured at pH 7.0; $\Delta H^{\circ\prime}_{rc}$, enthalpy change for the reaction center upon reduction of the oxidized protein; $\Delta S^{\circ\prime}_{rc}$, entropy change for the reaction center upon reduction of the oxidized protein; SHE, standard hydrogen electrode; 5-c, five coordinate; 6-c, six coordinate; HS, high spin; LS, low spin; RR, resonance Raman.

10.1021/bi0517943 CCC: $33.50
Published on Web 03/22/2006

peroxide at reasonable rates. This makes KatG an ideal model to study the structural requirements that enable a heme enzyme to efficiently catalyze H_2O_2 reduction and oxidation. We have recently shown that the tyrosine-to-phenylalanine mutation in *Synechocystis* KatG(Y249F) prevents cross-link formation (*7*) and converts bifunctional KatG to a monofunctional peroxidase that completely lost its catalatic acivity (*10*). The importance of an intact Trp-Tyr-Met adduct for catalase activity has also been demonstrated for KatG from *B. pseudomallei* (Y238F) (*11*) and *Mycobacterium tuberculosis* (Y229F) (*9*, *12*). Furthermore, the spectroscopic signatures of the redox intermediates of KatG(Y249F) significantly differed from those of the wild-type protein (*9*, *10*, *13*).

What role does the cross-link play in the redox chemistry of KatG, and is there a correlation between the redox chemistry and enzyme function? The indole ring of W122 is nearly coplanar and stacked above pyrrole ring B of heme *b* at a distance of about 3.7 Å, whereas Y249 is also within about 5.4 Å ($C^{\delta 2}$ to pyrrole ring A) of the heme periphery (Figure 1). Both W122 and Y249 are within the threshold for long-range electron transfer (*14*) and can be oxidized by compound I in the initial phase of autocatalytic cross-link formation (*9*). To address the question about the role of this adduct on the thermodynamics of the Fe^{3+}/Fe^{2+} couple of KatG and to elaborate differences in the redox chemistry of class I peroxidases, we have spectroelectrochemically (*15*, *16*) determined the temperature and pH dependence of the reduction potential of wild-type KatG and KatG(Y249F). When we started this work, there were only two articles about the $E^{\circ\prime}$ (Fe^{3+}/Fe^{2+}) of a catalase-peroxidase (*17*, *18*). *Mycobacterium tuberculosis* wild-type KatG and the variant S315T were reported to have a midpoint potential of ca. −50 mV at pH 7 (*17*) or −60 mV at pH 6 (*18*), which significantly differed from that of both C*c*P (−194 (*19*) and −182 mV (*20*)) and soybean APX (−160 mV) (*21*). However, the present work demonstrates that the redox properties within class I peroxidases are similar. Moreover, the $E^{\circ\prime}$ (Fe^{3+}/Fe^{2+}) value of KatG is shown to be -226 ± 10 mV, which is even more negative than that of C*c*P and APX. The inhibition of cross-link formation had no impact on the absolute value of $E^{\circ\prime}$, but on the relative enthalpic and entropic contributions to $E^{\circ\prime}$, as was determined by variable temperature experiments. With both proteins, the electron density at the heme iron decreased linearly with decreasing pH in the pH region 6−8.5.

MATERIALS AND METHODS

Mutagenesis, expression, and purification of wild-type KatG and KatG(Y249F) from *Synechocystis* PCC 6803 were described previously (*10*, *22*). All chemicals were reagent-grade.

To probe for the spectral signatures of ferrous proteins, ferric KatG or KatG(Y249F) was mixed in a glovebox with a small excess of sodium dithionite (Aldrich), either directly or from a freshly prepared anaerobic stock solution (50 mM phosphate buffer at pH 7.0 and at 25 °C). All solutions were made anaerobic by flushing with nitrogen gas (oxygen <3 ppm) and storing in a glovebox (Meca-Plex, Neugebauer) with a positive pressure of nitrogen (25 mbar). Electronic absorption spectra were determined in gastight cuvettes discharged from the glovebox (Zeiss Specord S10, Hitachi U-3000).

Spectroelectrochemistry. All experiments were carried out in a homemade OTTLE cell (*23*−*25*). The three-electrode configuration consisted of a gold minigrid working electrode (Buckbee-Mears, Chicago, IL), a homemade $Ag/AgCl/KCl_{sat}$ microreference electrode, separated from the working solution by a Vycor set, and a platinum wire as the counter electrode. The reference electrode was calibrated against a saturated calomel electrode before each set of measurements. All potentials are referenced to the SHE. Potentials were applied across the OTTLE cell with an Amel model 2053 potentiostat/galvanostat. The function of the OTTLE cell was checked by measuring the reduction potential of yeast iso-1-cytochrome *c* in conditions similar to those used in the present work. The $E^{\circ\prime}$ value corresponded to that determined by cyclic volammetry (+260 mV). A constant temperature was maintained by a circulating water bath, and the OTTLE cell temperature was monitored with a Cu-costan microthermocouple. UV−vis spectra were recorded using a Varian Cary C50 spectrophotometer.

The variable temperature experiments were performed using a nonisothermal cell configuration. The temperature of the reference electrode and the counter electrode was kept constant, whereas that of the working electrode was varied. For this experimental configuration $\Delta S^{\circ\prime}_{rc}$ is calculated from the slope of the $E^{\circ\prime}$ versus temperature plot, whereas $\Delta H^{\circ\prime}_{rc}$ is obtained from the Gibbs−Helmholtz equation $\Delta G^{\circ\prime}_{rc} = \Delta H^{\circ\prime}_{rc} - T\Delta S^{\circ\prime}_{rc} = -nFE^{\circ\prime}$, namely, from the slope of the plot of $E^{\circ\prime}/T$ versus $1/T$ (*26*). The Faraday constant F is 96485.31 $C \cdot mol^{-1}$, and n represents the number of electrons transferred by the redox couple.

All experiments were carried out under Argon over the 20−40 °C (wild-type) and 15−35 °C [KatG(Y249F)] range using 1 mL samples containing 0.02 mM protein in 50 mM phosphate buffer and 10 mM NaCl at pH 7.0, in the presence of 0.8 mM methyl viologen and 0.01 mM lumiflavine-3-acetate, indigo disulfonate, phenazine methosulfate, and methylene blue used as mediators. Nernst plots consisted of at least six points and were invariably linear, with a slope consistent with a one-electron reduction process. To determine the dependence of E'° on pH, the corresponding experiments were performed in 50 mM phosphate buffer and 10 mM NaCl at pH 6−8.5.

Application of conventional diffusion-controlled voltammetric techniques to KatG was hampered by its high molecular mass of 170 kDa.

RESULTS AND DISCUSSION

Figure 2 compares the electronic absorption spectra of ferric and ferrous wild-type KatG and KatG(Y249F). At pH 7.0, both the Soret (406 nm) and the CT1 bands (637 nm) of *Synechocystis* KatG suggest the presence of a 5-c HS heme coexisting with 6-c HS heme (*27*). The effect of the tyrosine-to-phenylalanine mutation in KatG(Y249F) on the spectral signature of both the ferric and ferrous forms is small. Recently reported resonance Raman data suggest that in KatG(Y249F) there is a small increase in 6-c LS heme (*28*). Upon reduction, the electronic absorption spectra are characteristic of 5-c HS hemes, again with a small increase of the 6-c LS species in ferrous KatG(Y249F) as suggested by

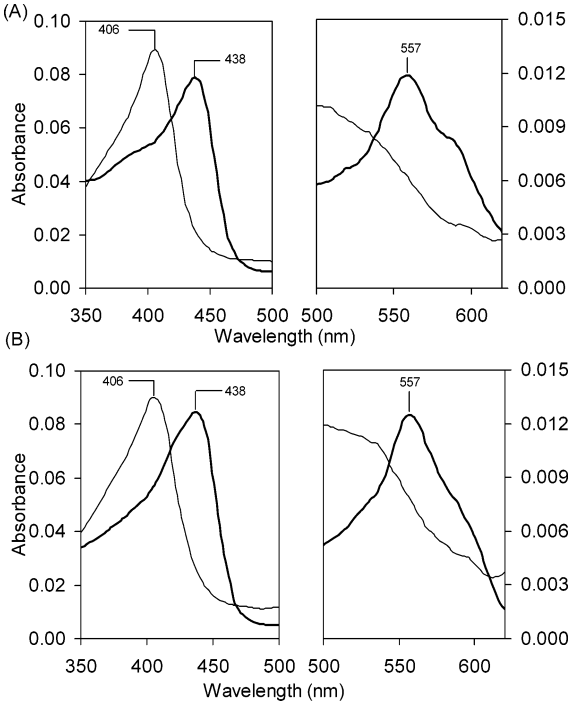

FIGURE 2: Spectral properties of oxidized and reduced wild-type KatG and KatG(Y249F). (A) 1 μM ferric (thin line) and ferrous (bold line) wild-type KatG. (B) 1 μM ferric (thin line) and ferrous (bold line) Y249F. Conditions: 50 mM phosphate buffer (pH 7.0) at 20 °C.

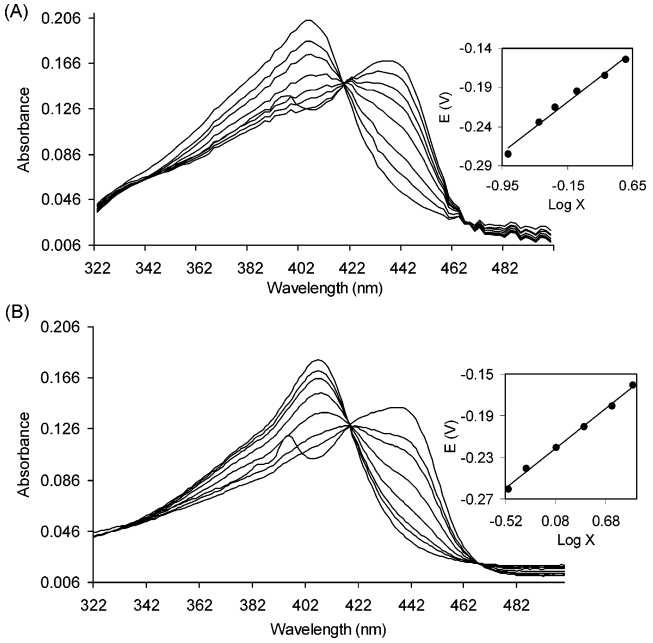

FIGURE 3: Electronic spectra of wild-type catalase-peroxidase from (A) *Synechocystis* PCC 6803 and (B) variant KatG(Y249F) obtained at various applied potentials. Spectra were recorded at 20 °C. The insets depict the corresponding Nernst plots, were X represents $[(A_{\lambda red}{}^{max} - A_{\lambda red})/(A_{\lambda ox}{}^{max} - A_{\lambda ox})]$ with $\lambda_{ox} = 406$ nm and $\lambda_{red} = 438$ nm (20 °C).

RR spectroscopy (*28*). Figure 2 shows the maximum spectral changes in the ferric to ferrous transition obtained upon addition of dithionite to both proteins. Typically, ferrous *Synechocystis* wild-type KatG and KatG(Y249F) have their Soret maxima at 438 nm and a prominent peak in the visible region at 557 nm with a shoulder around 580 nm (Figure 2).

A representative family of the spectra of wild-type KatG at various applied potentials is shown in Figure 3A. The midpoint reduction potential for the Fe^{3+}/Fe^{2+} couple, was determined from the corresponding Nernst plot (Figure 3A inset). At 25 °C and pH 7.0, the reduction potential of wild-type *Synechocystis* KatG is found to be -226 ± 10 mV, significantly lower than the published literature values of -50 and -60 mV obtained for KatG from *Mycobacterium tuberculosis* (*17*, *18*). The discrepancy is remarkable. It is very unlikely that the structure of *Synechocystis* KatG significantly differs from the four published KatG structures (*1*−*4*), which have more or less an identical heme pocket. The constellation of the six conserved key active-site residues (R119, W122, and H123 in the distal pocket and H259, W341, and D402 in the proximal pocket; *Synechocystis* numbering) as well as the peculiar covalent link (W122-Y249-M275) is in an almost identical arrangement in the four published KatG structures (Figure 1) (*1*−*4*). Nevertheless, at present, we cannot exclude the fact that the observed discrepancy in $E°'$ between *Synechocystis* and *M. tuberculosis* KatG is due to structural differences and/or different solution conditions.

The structure of the heme *b* moiety and the electrostatic interactions between the heme iron, the proximal histidine, and the immediate surrounding polypeptide matrix are similar in class I peroxidases (*1*−*6*). The reduction potentials for C*c*P was determined to be -194 (*19*) and -182 mV (*20*) and -160 mV (*21*) for soybean APX. It has been shown that the main determinant of $E°'$ (Fe^{3+}/Fe^{2+}) in class I peroxidases is the Asp−His−iron interaction at the proximal heme side (Figure 1) (*20*). The Asp−His interaction (H290 and D402 in Figure 1) serves to deprotonate the N^{δ} position of proximal histidine to provide a strong axial ligand with imidazolate character. In all class I peroxidases, this interaction between the proximal histidine and the aspartate is carefully optimized in strength and geometry. The H bond between D402 and the conserved tryptophan (W341) further restricts its position. Both crystal structures (*1*−*4*) and spectroscopic studies (*27*, *29*) demonstrate the existence of hydrogen bonds between D402 and H290 and W341 (Figure 1). The disruption of these interactions by mutations weakens the heme binding to the protein (much more pronounced than in C*c*P) affecting the UV−vis and RR spectral features as well as enzyme activity (*29*, *30*). The important role of the proximal Asp−His interaction has been documented with C*c*P. The disruption of the aspartate hydrogen bond to histidine in C*c*P had a dramatic effect on the redox potential of C*c*P (*20*). It shifted from -182 for wild-type C*c*P to -79 (D235N), -78 (D235A), and -113 mV (D235E). This effect is in agreement with the finding that a full imidazolate character of the proximal histidine enthalpically stabilizes the ferriheme by approximately 400 mV (*25*). Considering the almost identical geometry of the proximal triad Asp-His-Trp in class I peroxidases, it is unlikely that the midpoint potential of KatG is significantly different form that of wild-type C*c*P or APX. Thus, the published values can be hardly justified.

It was interesting to see that the disruption of the Met-Tyr-Trp adduct had no effect on the absolute value of $E°'$ (Fe^{3+}/Fe^{2+}) (Figure 3B and Table 1). This suggests that the complete loss of catalase activity in KatG(Y249F) does not have its origin in altered redox properties of the heme iron.

Table 1: Thermodynamic Parameters for $Fe^{3+} \rightarrow Fe^{2+}$ Reduction in Wild-Type *Synechocystis* KatG and the Variant Tyr249Phe[a]

protein	$E^{\circ\prime}$ (V)[b]	$\Delta H^{\circ\prime}_{rc}$ (kJ mol^{-1})	$\Delta S^{\circ\prime}$ (JK^{-1} mol^{-1})	$-\Delta H^{\circ\prime}_{rc}/F$ (V)	$T\Delta S^{\circ\prime}_{rc}/F$ (V)
WT KatG	−0.226	+17	−18	−0.176	−0.056
Tyr249Phe	−0.222	+9	−44	−0.093	−0.136
HRP-C	−0.306	+91	+210	−0.943	+0.648

[a] For comparison purposes, the thermodynamic parameters of HRP-C are presented. Average errors on $E^{\circ\prime}$, $\Delta H^{\circ\prime}_{rc}$, and $\Delta S^{\circ\prime}$ values are ±0.005 V, ±4 kJ mol^{-1}, and ±8 JK^{-1} mol^{-1}, respectively (*23*). [b] At 298.15 K and referred to the SHE. Often, the sum ($-\Delta H^{\circ\prime}_{rc}/F + T\Delta S^{\circ\prime}_{rc}/F$) does not exactly match $E^{\circ\prime}$ because the $\Delta H^{\circ\prime}_{rc}$ and $\Delta S^{\circ\prime}_{rc}$ values are rounded to the closest integer as a result of experimental error.

Moreover, it indicates that the iron−H290 bond strength and proximal interactions are similar in wild-type KatG and KatG(Y249F). This fits with RR data in the low-frequency region showing the two ν(Fe−Im) stretching modes of wild-type KatG and KatG(Y249F) at similar frequencies (*28*) suggesting that the mutation did not significantly affect the protein structure on the proximal side. Moreover, fluoride binding to the heme iron has also been shown to be similar in both proteins (*28*) indicating that the disruption of the Y249−W122 bond did not perturb the relative orientation of W122, which is important in the H-bond interaction with the fluoride ligand (*27*, *28*). We have to keep in mind that in wild-type KatG the positive charge of the sulfonium ion in the intact Met-Tyr-Trp adduct (Figure 1) may raise the redox potential of the covalently bound Y249 and W122 residues, the latter being nearly coplanar and stacked above the pyrrole ring B of the heme cofactor. In KatG(Y249F), the adduct and thus the positive charge are absent, suggesting a difference in the redox chemistry of W122. Whether this discrepancy has an effect on the redox chemistry of the heme iron and how it contributes to the observed absolute value of $E^{\circ\prime}$ (Fe^{3+}/Fe^{2+}) of KatG(Y249F) are unknown.

To get more insight into the mechanism of $E^{\circ\prime}$ modulation by the exchange of Y249, we investigated the temperature dependence of the reduction potential (Figure 4). This allows factorization of the corresponding enthalpic ($\Delta H^{\circ\prime}_{rc}$) and entropic ($\Delta S^{\circ\prime}_{rc}$) components. In both proteins, the oxidized state is enthalpically stabilized over the reduced state, but this effect is less pronounced in KatG(Y249F). The enthalpic contribution to the stabilization of the ferric form is much smaller in KatG compared to the class III peroxidase HRP-C: −0.176 versus −0.943 V (Table 1) (*23*). Moreover, the reduction of KatG leads to a decrease in entropy, whereas the reduction of native HRP-C is accompanied by a significant increase in entropy (Table 1) (*23*). In HRP-C, the enthalpy and entropy changes partially compensate, whereas in KatG, both contribute to the negative reduction potential.

The relative contributions of $\Delta H^{\circ\prime}_{rc}$ and $\Delta S^{\circ\prime}_{rc}$ to $E^{\circ\prime}$ of KatG and KatG(Y249F) are different, but the resulting midpoint potentials are identical. Such $H-S$ compensation has been found to be typical of changes in the reduction-induced reorganization of water molecules within the hydration sphere of the molecule (*31*). Indeed, Y249 is part of a KatG-specific loop (*1*−*4*) that constricts the access channel of H_2O_2 to the heme, which is characterized by a water lining (*1*−*4*). In KatG(Y249F), the entropic term yields the larger contribution to the negative reduction potential value.

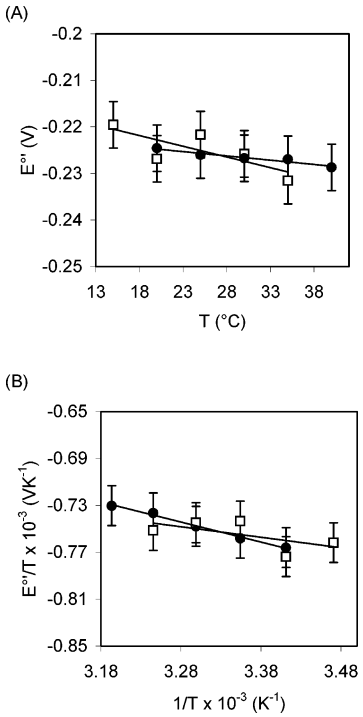

FIGURE 4: (A) Temperature dependence of the reduction potential and (B) $E^{\circ\prime}/T$ versus $1/T$ plots for wild-type KatG (●) and the variant, Y249F (□). The slope of the plots yields the $\Delta S^{\circ\prime}_{rc}/F$ and $-\Delta H^{\circ\prime}_{rc}/F$ values, respectively. Conditions: 0.02 mM protein in 50 mM phosphate buffer and 10 mM NaCl at pH 7.0.

It has been shown that $\Delta H^{\circ\prime}_{rc}$ is determined primarily by metal−ligand binding interactions and the electrostatics at the interface between the metal, the protein environment, and the solvent (*31*, *32*). In HRP-C, the large enthalpic term that contributes to the stabilization of the ferric form has been attributed to the basic character of the proximal histidine (because of its hydrogen bond interaction with the nearby aspartate), which stabilizes the higher oxidation state of the peroxidase, and to the polarity of the distal heme site maintained by the presence of water molecules involved in an extended network of hydrogen bonds (*23*). The main difference between class I peroxidases and HRP-C is the fact that the proximal aspartate (D247) in HRP acts as a H-bond acceptor of only the proximal histidine (H170) because a phenylalanine (F221) replaces the class I-typical proximal tryptophan (*33*). Thus, it is conceivable that in KatG the proximal His features a less pronounced anionic character than in HRP, which results in a smaller stabilization of the ferric heme. Unfortunately, no temperature-dependent data of $E^{\circ\prime}$ are available from C*c*P or APX to see whether these phenomena are KatG-specific or typical for all class I peroxidases. As in HRP, an extended H-bond network involving W122, H123, R119, etc. is also present in KatG (*1*−*4*, *29*). A highly conserved distal residue found only in KatG is an aspartate (D152) with its carboxyl oxygen pointing toward the heme pocket and H-bonded to two distal water molecules. However, an additional negative charge should stabilize the ferric form of the enzyme in which the heme core (iron plus nitrogen atoms) is positively charged (+1). A decrease in the enthalpic contribution to $E^{\circ\prime}$ is found upon cyanide binding to HRP, which causes a deep reorganization at the distal side because of water displacement, protonation of the distal histidine, which then forms an

hydrogen bond with the nitrogen atom of the bound cyanide, and the breaking of the proximal Asp−His bond (*23*). But even in the cyanide complex of HRP-C, the enthalpic term is much more positive compared to that of KatG. Another factor that could contribute to the decreased stabilization of the ferriheme in KatG compared to that in class III peroxidases is an overall decrease in the solvent accessibility of the heme, which also affects the reduction entropy (see below).

In the absence of structural information of ferrous KatGs, it is also difficult to interpret the entropic data. Generally, $\Delta S^{\circ\prime}_{rc}$ is mainly linked to oxidation state dependent changes in conformational degrees of freedom of the polypeptide chain and solvent reorganization effects (*31*, *32*). It is a common property of the vast majority of electron transport metalloproteins, irrespective of the nature of the metal center, that entropy is lost on reduction (*31*). In general, positive $\Delta S^{\circ\prime}_{rc}$ values are indeed associated with solvent exposed metal centers such as those of heme enzymes. In this respect, bifunctional KatG is similar to ET proteins and completely different from monofunctional HRP-C, and it is tempting to speculate whether this reflects different functional roles. KatG has a more deeply buried active site, and the proposed access route for H_2O_2 is provided by a channel similar to but longer and much more constricted than those in the other heme peroxidases (*1*−*4*). Similarly to monofunctional catalases (*34*), hydrogen peroxide enters the active site via an ordered matrix of oriented water molecules. A disruption of the H-bonding network or widening of the constriction by mutagenesis generally lowers the catalase and increases the peroxidase activity in both KatG and monofunctional catalases (*27*−*30*, *34*−*36*). It is reasonable to assume that because of the restricted access channel, reduction-induced solvent reorganization is strongly restricted. Moreover, the KatG-typical loop LL1, which includes Y249 and sets up part of the entrance and the surface of the access channel, is at one edge of the heme and connects the distal and proximal catalytic domains (Figure 1). Thus, Y249 anchors the LL1 loop by forming covalent bonds with Trp122 and Met275 to the distal side H-bond network thereby contributing to a very rigid protein structure that suppresses conformational changes of the protein backbone. The exchange of Y249 apparently readjusts the LL1 loop thereby increasing the 6-c LS species (*28*), which could be responsible for the even higher entropy loss in the reduction of KatG(Y249F).

Furthermore, we have elucidated the pH dependence of the reduction potential of both proteins in the pH range 6−8.5. At higher pH values it was not possible to prevent dioxygen binding to ferrous KatG (by extensive flushing with argon and/or by adding laccase and catalase to eliminate traces of O_2 and H_2O_2 (*37*)), whereas at acidic pH, *Synechocystis* KatG is known to be unstable. Figure 5 plots $E^{\circ\prime}$ as a function of pH. In both proteins, $E^{\circ\prime}$ decreased linearly with pH. For wild-type KatG, the slope of pH dependence was −44.8 mV/pH, whereas for KatG(Y249F), the slope was smaller (−35.5 mV/pH). These findings are in good agreement with the data reported for *M. tuberculosis* KatG (−52 mV/pH) (*18*). These values correspond to the binding of 1.5 (*Synechocystis* KatG) and 1.75 (*M. tuberculosis* KatG) protons per two electrons bound to wild-type KatGs, which are homodimeric proteins with two redox centers. The slightly smaller slope in KatG(Y249F) could be due to the small increase of 6-c LS hemes compared to the wild-type protein (*28*). It is known that distal heme ligands can decrease the pH dependence of the midpoint potential or even eliminate it, as was reported for chloride binding to myeloperoxidase (*38*). Thus, the small percentage of 6-c LS hemes in KatG(Y249F) (*28*) could be responsible for the observed difference with the wild-type protein. In any case, the pH dependence of $E^{\circ\prime}$ does not reflect the pH profile of the catalase activity of wild-type KatG, which exhibits a maximum around pH 6.5 (*22*, *40*). Moreover, in KatG(Y249F), the catalase activity is negligible, which also clearly emphasizes that fact that structural features other than simply the electron density at the heme iron are necessary for an enzyme to be catalatically active.

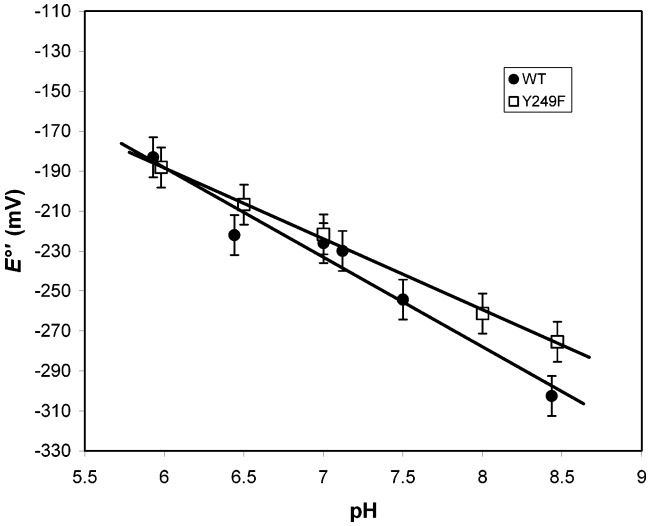

FIGURE 5: pH dependence of the reduction potential for wild-type KatG (●) and the variant, Y249F (□). Conditions: 0.02 mM protein in 50 mM phosphate buffer (pH 6−8.5) and 10 mM NaCl at 25 °C.

In summary, we have shown that catalase-peroxidases have class I peroxidase-type redox properties. This is plausible because only the ferric form is competent in H_2O_2 binding and reduction, which initiates both the peroxidase and catalase cycle (*39*). Disruption of the KatG-typical Met-Tyr-Trp does not alter the Fe^{3+}/Fe^{2+} midpoint potential of the heme iron as well as its dependence on pH. However, it converts the bifunctional enzyme to a monofunctional peroxidase (*10*). We note that the catalatic activity (i.e., the competence of H_2O_2 oxidation and dioxygen release) is not related to the redox properties of the Fe^{3+}/Fe^{2+} couple of the heme iron. Thermodynamically, H_2O_2 oxidation is not a problem for a heme enzyme because $E^{\circ\prime}(O_2/H_2O_2)$ is low, namely, + 280 mV (*39*). Because reduction potentials of heme proteins are controlled by structural factors (e.g., basicity of the proximal ligand and the pyrrole nitrogens or electrostatic interactions, etc.), it is reasonable to assume that the redox properties of the catalatically active intermediate compound I of wild-type KatG and Y249F are also similar. This suggests that other structural features enable an enzyme to oxidize H_2O_2 and release O_2. Recently, it has been demonstrated that catalase activity makes high demands on the substrate channel and protein integrity (*40*). Conformational changes and solvent reorganization during enzyme turnover, that is, during redox state transitions, are counterproductive because they would disrupt the molecular ruler

for the second hydrogen peroxide molecule. These functional imperatives could be responsible for the observed, rather modest, enthalpic and entropic changes (especially the latter) in KatG to HRP, which cannot oxidize H_2O_2. Unfortunately, the temperature dependence of $E^{\circ\prime}$ of other class I peroxidases and catalases is unknown, impeding a more comprehensive and comparative analysis.

REFERENCES

1. Yamada, Y., Fujiwara, T., Sato, T., Igarashi, N., and Tanaka, N. (2002) The 2.0 Å crystal structure of catalase-peroxidase from *Haloarcula marismortui*, *Nat. Struct. Biol. 9*, 691−695.
2. Carpena, X., Loprasert, S., Mongkolsuk, S., Switala, J., Loewen, P. C., and Fita, I. (2003) Catalase-peroxidase KatG of *Burkholderia pseudomallei* at 1.7 Å resolution, *J. Mol. Biol. 327*, 475−489.
3. Wada, K., Tada, T., Nakamura, Y., Kinoshita, T., Tamoi, M., Shigeoka, S., and Nishimura, K. (2002) Crystallization and preliminary X-ray diffraction studies of catalase-peroxidase from *Synechococcus* PCC 7942, *Acta Crystallogr., Sect. D 58*, 157−159.
4. Bertrand, T., Eady, N. A. J., Jones, J. N., Jesmin, Nagy, J. M., Jamart-Gregoire, B., Raven, E. L., and Brown, K. A. (2004) Crystal structure of *Mycobacterium tuberculosis* catalase-peroxidase, *J. Biol. Chem. 279*, 38991−38999.
5. Finzel, B. C., Poulos, T. L., and Kraut, J. (1984) Crystal structure of yeast cytochrome *c* peroxidase refined at 1.7-Å resolution, *J. Biol. Chem. 259*, 13027−13036.
6. Patterson, W. R., and Poulos, T. L. (1995) Crystal structure of recombinant pea cytosolic ascorbate peroxidase, *Biochemistry 34*, 4331−4341.
7. Jakopitsch, C., Kolarich, D., Petutschnig, G., Furtmüller, P. G., and Obinger, C. (2003) Distal side tryptophan, tyrosine and methionine in catalase-peroxidases are covalently linked in solution, *FEBS Lett. 552*, 135−140.
8. Donald, L. J., Krokhin, O. V., Duckworth, H. W., Wiseman, B., Deemagarn, T., Singh, R., Switala, J., Carpena, X., Fita, I., and Loewen, P. C. (2003) Characterization of the catalase-peroxidase KatG from *Burkholderia pseudomallei* by mass spectrometry, *J. Biol. Chem. 278*, 35687−35692.
9. Ghiladi, R. A., Knudsen, G. M., Medzihradszky, K. F., and Ortiz de Montellano, P. R. (2005) The Met-Tyr-Trp crosslink in *Mycobacterium tuberculosis* catalase-peroxidase (KatG): autocatalytic formation and effect on enzyme catalysis and spectroscopic properties, *J. Biol. Chem. 280*, 22651−22663.
10. Jakopitsch, C., Auer, M., Ivancich, A., Rüker, F., Furtmüller, P. G., and Obinger, C. (2003) Total conversion of bifunctional catalase-peroxidase (KatG) to monofunctional peroxidase by exchange of a conserved distal side tyrosine, *J. Biol. Chem. 278*, 20185−20191.
11. Singh, R., Wiseman, B., Deemagarn, T., Donald, L. J., Duckworth, H. W., Carpena, X., Fita, I., and Loewen, P. C. (2004) Catalase-peroxidases (KatG) exhibit NADH oxidase activity, *J. Biol. Chem. 279*, 43098−43106.
12. Yu, S., Girotto, S., Zhao, X., and Magliozzo, R. S. (2003) Rapid formation of compound II and a tyrosyl radical in the Y229F mutant of *Mycobacterium tuberculosis* catalase-peroxidase disrupts catalase but not peroxidase function, *J. Biol. Chem. 278*, 44121−44127.
13. Jakopitsch, C., Wanasinghe, A., Jantschko, W., Furtmüller, P. G., and Obinger, C. (2005) Kinetics of interconversion of ferrous enzymes, compound II and compound III, of wild-type *Synechocystis* catalase-peroxidase and Y249F, *J. Biol. Chem. 280*, 9037−9042.
14. Gray, H. B., and Winkler, J. R. (1996) Electron transfer in proteins, *Annu. Rev. Biochem. 65*, 537−561.
15. Dong, S., Niu, J., and Cotton, T. M. (1995) Ultraviolet/visible spectroelectrochemistry of redox proteins, *Methods Enzymol. 246*, 701−732.
16. Heineman, W. R., Norris, B. J., and Goelz, J. F. (1975) Measurement of enzyme $E^{\circ\prime}$ values by optically transparent thin layer electrochemical cells, *Anal. Chem. 47*, 79−84.
17. Wengenack, N. L., Lopes, H., Kennedy, M. J., Tavares, P., Pereira, A. S., Moura, I., Moura, J. J. G., and Rusnak, F. (2000) Redox potential measurements of the *Mycobacterium tuberculosis* heme protein KatG and the isoniazid-resistant enzyme KatG(S315T): insights into isoniazid activiation, *Biochemistry 39*, 11508−11513.
18. Zhang, Z., Chouchane, S., Magliozzo, R. S., and Rusling, J. F. (2002) Direct voltammetry and catalysis with *Mycobacterium tuberculosis* catalase-peroxidase, peroxidases, and catalase in lipid films, *Anal. Chem. 74*, 163−170.
19. Conroy, C. W., Tyma, P., Daum, P. H., and Erman, J. E. (1978) Oxidation-reduction potential measurements of cytochrome *c* peroxidase and pH dependent spectral transitions in the ferrous enzyme, *Biochim. Biophys. Acta 537*, 62−69.
20. Goodin, D. B., and McRee, D. E. (1993) The Asp-His-Fe triad of cytochrome *c* peroxidase controls the reduction potential, electronic structure, and coupling of the tryptophan free radical to the heme, *Biochemistry 32*, 3313−3324.
21. Jones, D. K., Dalton, D. A., Rosell, F. I., and Raven, E. L. (1998) Class I heme peroxidases: characterization of soybean ascorbate peroxidase, *Arch. Biochem. Biophys. 360*, 173−178.
22. Jakopitsch, C., Rüker, F., Regelsberger, G., Pircher, A., Dockal, M., Peschek, G. A., and Obinger, C. (1999) Catalase-peroxidase from the cyanobacterium *Synechocystis* PCC 6803: cloning, overexpression in *Escherichia coli*, and kinetic characterization, *Biol. Chem. 380*, 1087−1096.
23. Battistuzzi, G., Borsari, M., Ranieri, A., and Sola, M. (2002) Redox thermodynamics of the Fe^{3+}/Fe^{2+} couple in horseradish peroxidase and its cyanide complex, *J. Am. Chem. Soc. 124*, 26−27.
24. Battistuzzi, G., Bellei, M., Leonardi, A., Pieratelli, R., De Candia, A., Vila, A. J., and Sola, M. (2005) Reduction thermodynamics of the T1 Cu-site in plant and fungal laccases, *J. Biol. Inorg. Chem. 10*, 867−873.
25. Battistuzzi, G., Bellei, M., Borsari, M., Di Rocco, G., Ranieri, A., and Sola, M. (2005) Axial ligation and polypeptide matrix effects on the reduction potential of heme proteins probed on their cyanide adducts, *J. Biol. Inorg. Chem. 10*, 643−651.
26. Yee, E. L., Cave, R. J., Guyer, K. L., Tyma, P. D., and Weaver, M. J. (1979) A survey of ligand effects upon the reaction entropies of some transition metal redox couples, *J. Am. Chem. Soc. 101*, 1131.
27. Heering, H. A., Indiani, C., Regelsberger, G., Jakopitsch, C., Obinger, C., and Smulevich, G. (2002) New insights into the heme cavity structure of catalase-peroxidase: a spectroscopic approach to the recombinant *Synechocystis* enzyme and selected distal cavity mutants, *Biochemistry 41*, 9237−9247.
28. Santoni, E., Jakopitsch, C., Obinger, C., and Smulevich, G. (2004) Manipulating the covalent link between distal side tryptophan, tyrosine and methionine in catalase-peroxidases: an electronic absorption and resonance Raman study, *Biopolymers 74*, 46−50.
29. Santoni, E., Jakopitsch, C., Obinger, C., and Smulevich, G. (2004) Comparison between catalase-peroxidase and cytochrome *c* peroxidase. The role of the hydrogen-bond networks for protein stability and catalysis, *Biochemistry 43*, 5792−5802.
30. Jakopitsch, C., Regelsberger, G., Furtmüller, P. G., Rüker, F., Peschek, G. A., and Obinger, C. (2002) Engineering the proximal heme cavity of catalase-peroxidase, *J. Inorg. Biochem. 91*, 78−86.
31. Battistuzzi, G., Borsari, M., Di Rocco, G., Ranieri, A., and Sola, M. (2004) Enthalpy/entropy compensation phenomena in the reduction thermodynamics of electron transport metalloproteins, *J. Biol. Inorg. Chem. 9*, 23−26.
32. Battistuzzi, G., Borsari, M., Sola, M., and Francia F. (1997) Redox thermodynamics of the native and alkaline forms of eukaryotic and bacterial class I cytochromes *c*, *Biochemistry 36*, 16247−16258.
33. Gajhede, M., Schuller, D. J., Henriksen, A., Smith, A. T., and Poulos, T. L. (1997) Crystal structure of horseradish peroxidase C at 2.15 Å resolution, *Nat. Struct. Biol. 4*, 1032−1038.
34. Nicholls, P., Fita, I., and Loewen, P. C. (2001) Enzymology and structure of catalases, *Adv. Inorg. Chem. 51*, 51−106.
35. Mate, M. J., Zamocky, M., Nykyri, L. M., Herzog, C., Alzari, P. M., Betzel, C., Koller, F., and Fita, I. (1999) Structure of catalase-A from *Saccharomyces cerevisiae*, *J. Mol. Biol. 286*, 13−149.
36. Mate, M. J., Sevinc, M. S., Hu, B., Bujons, J., Bravo, J., Switala, J., Ens, W., Loewen, P. C., and Fita, I. (1999) Mutants that alter the covalent structure of catalase hydroperoxidase II from *Escherichia coli*, *J. Biol. Chem. 274*, 27717−27725.

37. Millis, C. D., Cai, D., Stankovich, M. T., and Tien, M. (1989) Oxidation−reduction potentials and ionization states of extracellular peroxidases from the lignin-degrading fungus *Phanerochaete chrysosporium*, *Biochemistry 28*, 8484−8489.
38. Ikeda-Saito, M., and Prince, R. C. (1985) The effect of chloride on the redox and EPR properties of myeloperoxidase, *J. Biol. Chem. 260*, 8301−8305.
39. Dunford, H. B. (1999) *Heme Peroxidases*, Wiley-VCH, New York.
40. Jakopitsch, C., Droghetti, E., Schmuckenschlager, F., Furtmüller, P. G., Smulevich, G., and Obinger, C. (2005) Role of the main access channel of catalase-peroxidase in catalysis, *J. Biol. Chem. 280*, 42411−42422.

BI0517943